The Astrophysical Journal, 746:98 (11pp), 2012 February 10 doi:10.1088/0004-637X/746/1/98
© 2012. The American Astronomical Society. All rights reserved. Printed in the U.S.A.

CONVERGENCE STUDIES OF MASS TRANSPORT IN DISKS WITH GRAVITATIONAL INSTABILITIES. I. THE CONSTANT COOLING TIME CASE

Scott Michael[1], Thomas Y. Steiman-Cameron[1], Richard H. Durisen[1], and Aaron C. Boley[2]
[1] Astronomy Department, Indiana University, Bloomington, IN 47405, USA; scamicha@astro.indiana.edu, tomsc@astro.indiana.edu, durisen@astro.indiana.edu
[2] Department of Astronomy, University of Florida, Gainesville, FL 32611, USA; aaron.boley@gmail.com
Received 2011 March 25; accepted 2011 December 9; published 2012 January 27

ABSTRACT

We conduct a convergence study of a protostellar disk, subject to a constant global cooling time and susceptible to gravitational instabilities (GIs), at a time when heating and cooling are roughly balanced. Our goal is to determine the gravitational torques produced by GIs, the level to which transport can be represented by a simple α-disk formulation, and to examine fragmentation criteria. Four simulations are conducted, identical except for the number of azimuthal computational grid points used. A Fourier decomposition of non-axisymmetric density structures in $\cos(m\phi)$, $\sin(m\phi)$ is performed to evaluate the amplitudes A_m of these structures. The A_m, gravitational torques, and the effective Shakura & Sunyaev α arising from gravitational stresses are determined for each resolution. We find nonzero A_m for all m-values and that A_m summed over all m is essentially independent of resolution. Because the number of measurable m-values is limited to half the number of azimuthal grid points, higher-resolution simulations have a larger fraction of their total amplitude in higher-order structures. These structures act more locally than lower-order structures. Therefore, as the resolution increases the total gravitational stress decreases as well, leading higher-resolution simulations to experience weaker average gravitational torques than lower-resolution simulations. The effective α also depends upon the magnitude of the stresses, thus $\alpha_{\rm eff}$ also decreases with increasing resolution. Our converged $\alpha_{\rm eff}$ is consistent with predictions from an analytic local theory for thin disks by Gammie, but only over many dynamic times when averaged over a substantial volume of the disk.

Key words: accretion, accretion disks – protoplanetary disks – stars: formation

Online-only material: color figures

1. INTRODUCTION

Detailed three-dimensional (3D) hydrodynamic modeling of protostellar disks has provided considerable insight into the physical and thermal states of these disks. However, computing resources limit these studies to durations spanning timescales much shorter than a disk's evolutionary lifetime. The level of spatial resolution, and hence temporal resolution due to the Courant condition, can play a deterministic role in interpretations of calculations; while lower resolutions allow more extensive spatial and temporal studies, this benefit can come at the sacrifice of important physics. Convergence studies provide a means of deriving important outcomes while assessing the resolution needed to determining these outcomes.

In contrast to sophisticated calculations that include detailed physics, approaches exist that replace detailed physics with statistical parameters that encapsulate this physics. This allows for calculations covering much longer time frames. Both detailed and parametric approaches can play important roles in broadening our understanding of complex nonlinear systems, provided a connection between the detailed physics and statistical parameters can be demonstrated and understood. In what follows, we perform convergence tests on hydrodynamical disk simulations to examine the applicability of an α-disk formulation (Shakura & Sunyaev 1973) to the evolution of protostellar disks subject to gravitational instabilities (GIs).

GIs can play an important, and at times dominant, role in driving the structural evolution of protostellar disks (for reviews, see Durisen et al. 2005, 2007). Thermal processes play the primary role in regulating the amplitude and outcome of these instabilities (Pickett et al. 1998, 2000, 2003; Nelson et al. 1998, 2000; Mejía et al. 2005). A disk's susceptibility to GIs can be parameterized by the Toomre Q-parameter (Toomre 1981); $Q = c_s\kappa/\pi G\Sigma$, where c_s is the sound speed, κ is the epicyclic frequency ($\sim$ the rotation frequency Ω in a nearly Keplerian disk), and Σ is the disk surface mass density. For $Q \lesssim 1.7$, small density perturbations in a disk grow exponentially on a timescale comparable to the rotation period (Durisen et al. 2007). These perturbations manifest themselves as multi-arm spirals with a predominantly trailing pattern that transports angular momentum outward by gravitational torques (Larson 1984; Boss 1984; Durisen et al. 1986; Papaloizou & Savonije 1991; Laughlin & Bodenheimer 1994; Nelson et al. 1998; Pickett et al. 1998).

Numerous studies have shown that thermal physics controls GI amplitudes by a *balance* of heating and cooling (e.g., Tomley et al. 1991, 1994; Pickett et al. 1998, 2000, 2003; Gammie 2001; Boss 2002; Rice et al. 2003; Mejía et al. 2005; Boley et al. 2006, 2007a; Stamatellos & Whitworth 2008; Cossins et al. 2009). Heating by GIs tends to increase c_s, thus increasing Q. If disk heating persists, the instability will be suppressed once Q becomes sufficiently large. On the other hand, radiative cooling tends to oppose the increase in Q by lowering c_s. In this way, heating and cooling can reach a rough overall balance at nonlinear wave amplitude. GI activity can sustain this balance at a relatively constant, but unstable, value of Q (Paczynski 1978; Lin 1981; Goldreich & Lynden-Bell 1965), and the disk can exist in a state of quasi-equilibrium. In this state, cooling is balanced by heating arising from the inward flow of matter and shocks induced by the GIs (Gammie 2001; Lodato & Rice 2004; Rice et al. 2005; Boley et al. 2006; Cossins et al. 2009; Vorobyov 2010).

We note here a caution on semantics. GIs in disks commonly manifest themselves as non-axisymmetric density structures whose strengths can be characterized by a Fourier decomposition of the density in terms of $\sin m\phi$ and $\cos m\phi$, where m

is the order of the Fourier term and ϕ is the usual cylindrical coordinate. While discrete coherent spiral waves seen in these disks may well be correctly thought of as eigenmodes, particularly at low m-values, the analysis necessary to confirm that these structures are, in fact, truly modes is generally lacking. Power in a specific m-value does not imply the existence of that mode, nor does it necessarily represent the strength of a mode that truly exists. Indeed, a disk with a *single* $m = 2$ eigenmode growing to nonlinear amplitudes will exhibit power at all even values of m. A disk with *two* nonlinear eigenmodes of $m = 2$ and 3 will exhibit power at all m-values. For this reason, in the balance of this paper we will avoid referring to the Fourier terms as modes, but rather will refer to them as Fourier structures or components. The term *mode* will be reserved for those cases where eigenmodes are known, or strongly suspected, to exist.

Fully nonlinear hydrodynamic simulations of low-Q disks show that multiple modes can become unstable in the linear regime (Nelson et al. 1998; Pickett et al. 1998; Lodato & Rice 2004; Boley et al. 2006; Cossins et al. 2009). Even if the initial growth is dominated by one mode, numerous modes usually appear in the nonlinear regime. As a consequence, if a disk achieves a quasi-steady balance between heating and cooling, referred to as the *asymptotic state*, then power will exist at all m-values resolved by a given numerical method (Mejía et al. 2005; Boley et al. 2006). In the asymptotic state, GI-active disks develop overlapping density structures of different strengths, geometries, and coherence that pervade the entire disk (e.g., Pickett et al. 2003; Mejía et al. 2005; Boley et al. 2006). These structures provide a possible bridge between the detailed physics of GIs and the viscous transport parameter α (Gammie 2001). Here convergence studies are important because higher-order modes dissipate energy on shorter wavelengths than lower-order modes; the mix of low- and high-order azimuthal density structures available to a disk is set by the resolution of the simulation.

Shakura & Sunyaev (1973) proposed turbulence as the primary source of effective viscosity in gas disks and parameterized turbulent transport in a steady-state disk with the parameter α (see also Pringle 1981). In this case, the kinematic viscosity is defined by $\nu = \alpha c_s H$, where c_s is the sound speed and H is the disk height. The source of the turbulence in their α-disk formulation is unspecified. Although their original work was directed toward X-ray bright accretion disks around black holes, this heuristic approach has proven fruitful in many astrophysical situations by allowing for analytic solutions and relatively easy numerical modeling over time-spans inaccessible to detailed modeling. The α formalism makes no assumption about the nature of the angular momentum transport, only that *angular momentum transport and heating are dominated by local processes*. Lin & Pringle (1987, 1990) were among the first to suggest that GI-induced transport could be described within a viscous framework. However, the validity of an α-disk picture requires self-consistency of local energy dissipation. The locality of dissipation in GI-active disks has not been thoroughly tested and remains an open question (Lodato & Rice 2004, 2005; Boley et al. 2006).

In fact, several studies support the idea that angular momentum transport by GIs in real disks is, in many important respects, an intrinsically global phenomenon and cannot be properly treated by a local α-like prescription (Laughlin & Rozyczka 1996; Balbus & Papaloizou 1999; Lodato & Rice 2005; Mejía et al. 2005; Boley et al. 2006; Cai et al. 2008). This almost certainly applies to the embedded phase of both high- and low-mass stars when infall from the collapsing protostellar cloud feeds mass into the disk at a rapid rate (e.g., Yorke et al. 1993; Laughlin & Bodenheimer 1994; Yorke & Bodenheimer 1999; Vorobyov & Basu 2005, 2006; Kratter et al. 2010; Walch et al. 2010). However, despite the long-distance nature of gravitational torques, theoretical and numerical results suggest that in protostellar disks where heating and cooling are in rough balance, it may be valid to represent GI-induced transport by an *effective viscosity*, as if it were a local process (Gammie 2001; Lodato & Rice 2004; Rice et al. 2005; Cossins et al. 2009; Vorobyov 2010). In particular, multiple studies suggest that an effective α-viscosity may be consistent with transport in GI-active disks for a disk-to-star mass ratio $M_d/M_* \leqslant 0.2$–0.3; GI-active disks in systems with larger M_d/M_* are dominated by lower-order modes that act in a more global sense and thus cannot be well represented by an α-approach (Lodato & Rice 2004; Cossins et al. 2009; Vorobyov 2010). We note, however, that these studies all assumed a *local cooling time*, $t_{\rm cool}\Omega$ = constant, where $t_{\rm cool}$ is defined by the rate at which cooling decreases the disk's internal energy density ϵ by $d\epsilon/dt = \epsilon/t_{\rm cool}$. In contrast, we and our collaborators use either a *global cooling time*, $t_{\rm cool}$ = constant (e.g., Pickett et al. 2003; Mejía et al. 2005, this paper), or use realistic opacities (e.g., Mejía 2004; Cai et al. 2006, 2008; Boley et al. 2006, 2007a; Boley 2009) which lead to something in between $t_{\rm cool}$ = constant and $t_{\rm cool}\Omega$ = constant. The review by Durisen et al. (2007) discusses some consequences of these various choices. There is a tendency for $t_{\rm cool}\Omega$ = constant to bias a disk toward behavior like that of a steady-state α-disk.

Gammie (2001) derived an effective α for the case of a thin gravitationally unstable disk where the heating caused by GIs was balanced by the local cooling rate (see also Pringle 1981). Assuming a local cooling time of $t_{\rm cool}\Omega$ = constant, Gammie found

$$\alpha_{\rm eff} = \left[\gamma(\gamma - 1)\frac{9}{4}\Omega t_{\rm cool}\right]^{-1}, \quad (1)$$

where γ is the two-dimensional (2D) adiabatic index. The 2D index relates to the 3D adiabatic index, Γ, by $\gamma = (3\Gamma - 1)/(\Gamma + 1)$ for a non-self-gravitating disk and $\gamma = 3 - 2/\Gamma$ for a strongly self-gravitating disk. Lodato & Rice (2004) derived a similar result when considering 3D protoplanetary disks. Fully 3D simulations (e.g., Lodato & Rice 2004; Cossins et al. 2009) suggest that, at least in the case of imposed $t_{\rm cool}\Omega$ = constant cooling, $\alpha_{\rm eff}$ roughly converges to the value given by Equation (1).

In what follows, we address these and related questions using a grid-based, finite-difference 3D hydrodynamics code with self-gravity to follow the evolution of a protostellar disk with a constant cooling time and subject to GIs. We examine how grid resolution affects the amplitude distribution of azimuthal density structures arising from GIs, the gravitational torques arising from these structures, the effective α, and the extent to which transport can be represented by an α-disk formulation. A mesh convergence study provides a common approach to balancing accuracy and computing resources. It permits an assessment of whether or not convergence occurs and what resolution is required. In the following sections, we follow the evolution of a disk subject to GIs using grids with four different resolutions in the azimuthal direction. The number of azimuthal elements used in simulations may be particularly important because higher azimuthal resolution allows power in non-axisymmetric density structures to spread to higher-order modes that behave more locally. Although full convergence

testing eventually requires investigation of the radial and vertical resolution in our cylindrical grid, these tests are expensive and will be left to a future paper. We suspect that the azimuthal direction is most important to test first because it is non-axisymmetry that produces the torques leading to mass and angular momentum transport. We test this by examining the amplitude in various m-values to see how they are affected by the choice of grid. In the process, we report the results of a convergence study designed to determine whether GI-active disks, chaotic by nature, achieve statistical equilibrium. If this is the case, we investigate how closely these disks approximate Equation (1) from Gammie (2001) and examine the distribution of $\alpha_{\rm eff}$.

The remainder of this paper is organized as follows. Section 2 provides the details of the numerical approach and defines the models. An analysis of the azimuthal density structures of the simulations is found in Section 3.1, and the gravitational torques arising from these structures follows in Section 3.2. Effective converged alphas are discussed in Section 3.3. Section 3.4 deals with the degree to which selected grid sizes lead to results consistent with convergence. Fragmentation is discussed in Section 3.5. A summary of results is found in Section 4.

2. HYDRODYNAMICAL SIMULATIONS

Simulations were conducted with the 3D hydrodynamics code used by the Indiana University Hydrodynamics Group in several previous studies (Pickett et al. 1998, 2000; Mejía 2004; Mejía et al. 2005; Boley et al. 2006; Cai et al. 2008). This code uses a second-order, explicit, Eulerian scheme to solve Poisson's equation, an ideal gas equation of state, and the equations of hydrodynamics in conservative form on a uniform cylindrical grid. The code assumes mirror symmetry about the equatorial plane. It includes both self-gravity and artificial viscosity; the latter serves to mediate shocks. Source and flux terms (Norman & Winkler 1986) are computed separately in an explicit, second-order time integration (van Albada et al. 1982; Christodoulou 1991; Yang 1992).

Initial conditions for the disk's structure and thermodynamic state were set using an equilibrium star plus disk model generated by a modified Hachisu (1986) self-consistent field relaxation method (Pickett et al. 1996, 2003; Mejía 2004; Mejía et al. 2005; Cai et al. 2006). Here the density and angular momentum distributions are iteratively solved, using the specified equation of state, until convergence is achieved. This equilibrium disk was given random cell-to-cell $\sim 10^{-4}$ density perturbations to seed growth of GIs. The resultant marginally unstable disk served as the initial disk for the simulation.

Because this is a polytropic disk with an idealized cooling time, only the ratio of disk to stellar mass, given here by 0.153, is specified. In what follows, quantities specified with real physical units are derived assuming a 1 $M_\odot$ central star and a 0.153 $M_\odot$ disk. In this case, the outer rotation period (ORP) is defined at $r = 33$ AU and one ORP $\approx$ 214 yr. The disk has an initial surface density $\Sigma \sim r^{-1}$, with initial inner and outer radii of 2.3 and 40 AU, respectively. The construction of these initial equilibrium disk models is discussed in Pickett et al. (2003) and Mejía et al. (2005).

We assume an equation of state $P = (\gamma - 1)\epsilon$, where P is the pressure, ϵ is the internal energy density, and γ is the ratio of specific heats, given here by $\gamma = 5/3$. As discussed in Boley et al. (2007b), the rotation states of H_2 are probably not excited in the cold outer parts of the disk (>10 AU); so $\gamma = 5/3$ is an appropriate choice. The model disks are cooled by decreasing their internal energy according to the prescription $d\epsilon/dt = \epsilon/t_{\rm cool}$, where $t_{\rm cool}$ is the global cooling time, which is set to 2 ORPs everywhere.

Table 1
Q, Fourier Amplitudes, α, and $\dot{M}$

$l_{\rm max}$	$Q_{\rm avg}$	$\langle A_{\rm tot}\rangle$	$\langle A_{2-7}\rangle/\langle A_{\rm tot}\rangle$	$\alpha_{\rm avg}$	$\lvert\dot{M}\rvert_{\rm avg}$ ($M_\odot$ yr^{-1})
64	1.26	1.96	0.76	0.069	8.9×10^{-7}
128	1.24	1.91	0.62	0.044	3.7×10^{-7}
256	1.39	1.83	0.54	0.026	2.5×10^{-7}
512	1.48	1.95	0.49	0.020	2.4×10^{-7}
∞			0.43	0.017	

Notes. All quantities are time-averaged over 12–18 ORPs. $Q_{\rm avg}$, $\alpha_{\rm avg}$, and $\lvert\dot{M}\rvert_{\rm avg}$ are also spatially averaged over 10–40 AU. The entries for "∞" are based on Richardson extrapolation, as explained in the text.

The initially unstable disk model passed through several phases of evolution (see also Pickett et al. 2003; Mejía et al. 2005). During the initial axisymmetric phase, which lasts several ORPs, the disk cools and contracts. The contraction is small radially but dramatic in the vertical direction. Around 3–4 ORPs, the instabilities begin to grow to nonlinear amplitudes, and the disk then undergoes a strong burst of GIs that predominantly manifest themselves in a few discrete global spiral modes. The disk expands violently during the burst phase, producing a significant rearrangement of the disk's mass distribution on a timescale of a few ORPs. This is then followed by a period of several ORPs where heating temporarily washes out some of the non-axisymmetry in the disk. Finally, following this transition phase, the disk settles into a quasi-steady, long-lived asymptotic phase of sustained GI activity over a large part of the disk, with an overall balance of heating and cooling.

Simulations were run with four different angular resolutions, with grid sizes in cylindrical coordinates (r, ϕ, z) of $(j_{\rm max}, k_{\rm max}, l_{\rm max}) = (512,64,64)$, $(512,64,128)$, $(512,64,256)$, and $(512,64,512)$. For reference, the radius $r = 33$ AU at which the ORP is defined is at radial cell $j = 200$. The radial grid extends to 512 to accommodate disk expansion during outburst. Because of the computational overhead associated with running each simulation starting from $t = 0$, the $l_{\rm max} = 128$ simulation was run through the axisymmetric, burst, and transition phases. Simulations using $l_{\rm max} = 64$, 256, and 512 all begin by a linear interpolation of the $l_{\rm max} = 128$ simulation to higher or lower azimuthal resolution at 9.6 ORPs, near the end of the transition phase. Although this strategy saves a large amount of computational time, it limits the scope of the analysis to the asymptotic phase. By 12 ORPs, all four disks appear to have transitioned to the asymptotic state, e.g., they all display roughly steady $Q(r)$ profiles starting at ~12 ORPs. All simulations were run through ~18 ORPs.

Figure 1 shows the Toomre Q, as a function of radius, for all four simulations at $t \sim 18$ ORPs. Table 1 lists $Q_{\rm avg}$, the arithmetic mean of Q for each of the asymptotic disks, time-averaged from 12–18 ORPs, and spatially averaged over 10–40 AU. From ~12–50 AU, $Q \sim 1.0$–1.4 and thus the disk is subject to GIs over this full range.

3. RESULTS AND DISCUSSION

3.1. Non-axisymmetric Structure

In the asymptotic state, GI-active disks develop complex density structures arising from the superposition of

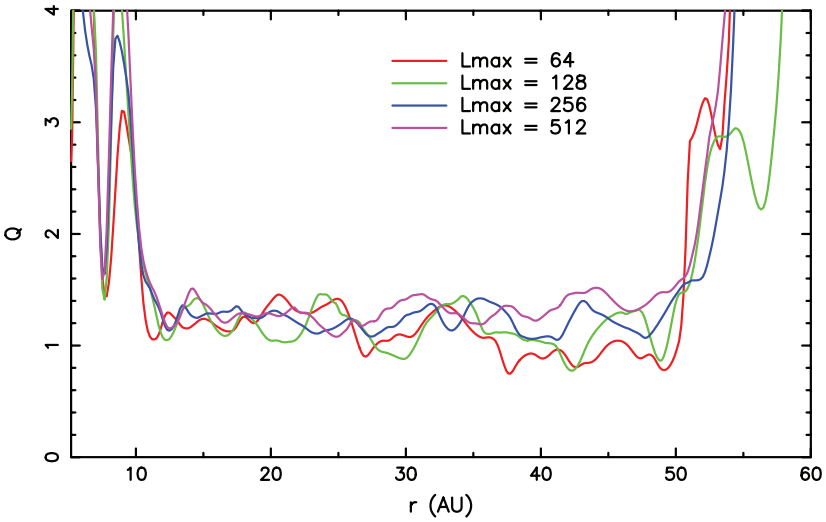

Figure 1. Azimuthally averaged mid-plane Toomre Q distribution vs. radius for each of the four resolutions at $t \sim 18$ ORPs.
(A color version of this figure is available in the online journal.)

non-axisymmetric modes in the disk. Since the number of modes accessible to the disk depends on the azimuthal resolution (Shannon 1984), we expect that higher-resolution simulations will exhibit non-axisymmetric amplitude in higher-order modes inaccessible at lower resolution, and these higher-order modes will behave more locally.

Figure 2 shows mid-plane and radial densities at $t \sim 18$ ORPs for the $l_{\max} = 64$, 128, 256, and 512 simulations. It is readily apparent that the character of the non-axisymmetric density structures differs with resolution. One can clearly see that the lower-resolution simulations, i.e., $l_{\max} = 64$ and 128, have primarily low-order structures with $m = 2$ and 3 dominating. In contrast, the higher-resolution simulations have much more fine structure, and the low-order m-values no longer dominate. The lower-resolution (smaller $l_{\max}$) simulations display longer wavelength spiral structures, with larger amplitudes and more coherence than those seen in higher-resolution simulations. Higher angular resolution allows non-axisymmetric structures to grow in higher-order azimuthal m-values, as demonstrated by a Fourier decomposition of the density. The strengths of these components are given by their global Fourier amplitudes,

$$A_m = \frac{\left(a_m^2 + b_m^2\right)^{1/2}}{\pi \int \rho_o \varpi \, d\varpi \, dz}, \tag{2}$$

where

$$a_m = \int \rho \cos(m\phi) \varpi \, d\varpi \, dz d\phi, \tag{3a}$$

$$b_m = \int \rho \sin(m\phi) \varpi \, d\varpi \, dz d\phi. \tag{3b}$$

Here, ρ_o is the axisymmetric component of the density. In what follows, A_m is averaged over time to suppress fluctuations on the dynamic timescale due to the chaotic nature of GIs in the asymptotic phase. In particular, $\langle A_{\rm tot} \rangle$ will represent the power over the radial range 10–40 AU, summed from $m = 2$ to $l_{\max}/2$ and averaged over the time range 12–18 ORPs. The Fourier amplitudes cannot be measured at resolutions smaller than $l_{\max}/2$, therefore A_m is limited to modes $m \leqslant l_{\max}/2$. Because the central star is artificially fixed to the grid center, the $m = 1$ mode may not be accurately treated. For this reason, it is excluded from $\langle A_{\rm tot} \rangle$. As discussed below in Section 3.2, we expect this exclusion to have minimal impact on the results of this work.

Previous studies have shown that disks in the asymptotic state have power at all resolvable m-values (Lodato & Rice 2004; Mejía et al. 2005; Boley et al. 2006; Cossins et al. 2009). This can be seen in Figure 3, where $\log\langle A_m \rangle$ is displayed as a function of $\log(m)$. For all resolutions, components with the highest global amplitudes are those with low m-values; $m = 2$–6 are labeled. In what follows, the term "low order" will refer to Fourier components with $m < 8$. Table 1 lists $\langle A_{\rm tot} \rangle$ along with $\langle A_{2-7} \rangle / \langle A_{\rm tot} \rangle$, the fraction of the total power falling into low-order ($m = 2$–7) azimuthal structures, for each resolution. We identify $m = 2$–7 as representing amplitude in the low-order modes, i.e., coherent structure that is global in character. Again $m = 1$ is excluded due to the fixed central star. This determination of m-range was made by considering the radial range over which the mode is most effective in transporting angular momentum, i.e., from the inner Linblad resonance to the outer Linblad resonance, and comparing it to the disk scale height. These quantities are roughly equal for $m = 7$; for lower-order modes the radial range exceeds the scale height. The vertical dotted line in Figure 3 corresponds with $m = 7$. While the total power is approximately independent of resolution, $\langle A_{\rm tot} \rangle \sim 1.90$, the distribution of this power amongst m-values shows marked differences. In particular, the fractional power in lower-order m-values decreases monotonically with increasing resolution. Over three-quarters of $\langle A_{\rm tot} \rangle$ resides in $m = 2$–7 for the $l_{\max} = 64$ simulation, while approximately half resides in these m-values when $l_{\max} = 512$.

The shift of power from lower-order to higher-order azimuthal structure as the resolution of the computational grid is increased arises from the fact that, while $\langle A_{\rm tot} \rangle$ is approximately independent of $l_{\max}$, the number of degrees of freedom available for this power, $l_{\max}/2$, increases linearly with the resolution. Thus, amplitude is naturally spread from lower order to higher order as the available m-values increase. Indeed, even if the disk is dominated by a few low-order modes at the time of outburst, this power spreads to all m-values in the nonlinear regime (for example Laughlin et al. 1997, 1998; Laughlin & Rozyczka 1996).

Given how the non-axisymmetric amplitude distribution depends on the azimuthal resolution, we must examine what resolution is sufficient to properly capture the evolution of these

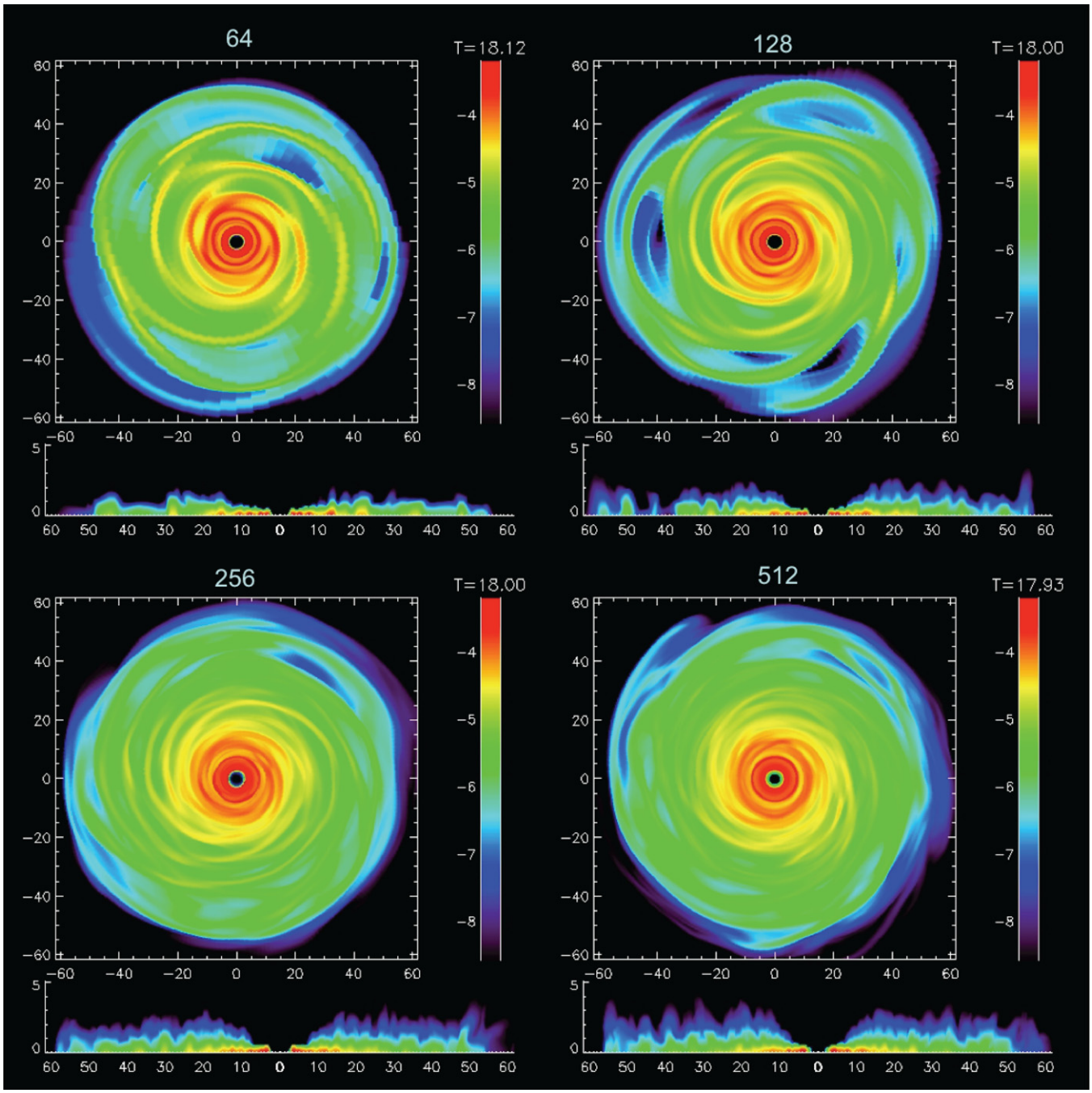

Figure 2. Mid-plane disk densities at $t \sim 18$ ORPs for simulations with 64, 128, 256, and 512 azimuthal grid elements. The simulations differ only in the number of azimuthal zones used in the calculations. Densities out of the plane, along an azimuthal cut through the disk, are displayed below the face-on views. The color scale is logarithmic, and axis units are AU.

disks. Table 1 shows that while the fractional power in lower-order m-values decreases with each doubling of $l_{\max}$, the amount of change in going from $l_{\max} = 256$ to 512 is significantly less than the change going from $l_{\max} = 64$ to 128, with a strong suggestion that this diminution will not proceed much further with higher azimuthal resolution. Indeed, a Richardson extrapolation (Press et al. 1992) of the tabulated values of $\langle A_{2-7}\rangle/\langle A_{\rm tot}\rangle$ suggests a limiting value of $\langle A_{2-7}\rangle/\langle A_{\rm tot}\rangle \sim 0.43$ for increasingly higher resolutions. This is displayed graphically in Figure 4, where the fractional amplitude in lower orders is plotted against the normalized grid spacing for each value of $l_{\max}$. The grid spacing is normalized such that spacing of the $l_{\max} = 512$ grid equals unity. Convergence occurs as the normalized spacing goes to zero. The Richardson extrapolation value of $\langle A_{2-7}\rangle/\langle A_{\rm tot}\rangle = 0.43$ is plotted at a normalized grid spacing equal to zero.

3.2. Gravitational Torques

Low-order spiral modes in the density distribution have longer wavelengths that, if coherent in radius, have longer lever arms to produce torques, while high-order modes have relatively short wavelengths which, particularly if they lack coherence, can cancel each other out and produce more localized effects. The finding that the fractional power in high-order structure increases with resolution, while the total power stays the same, leads to the expectation that the gravitational torques in the

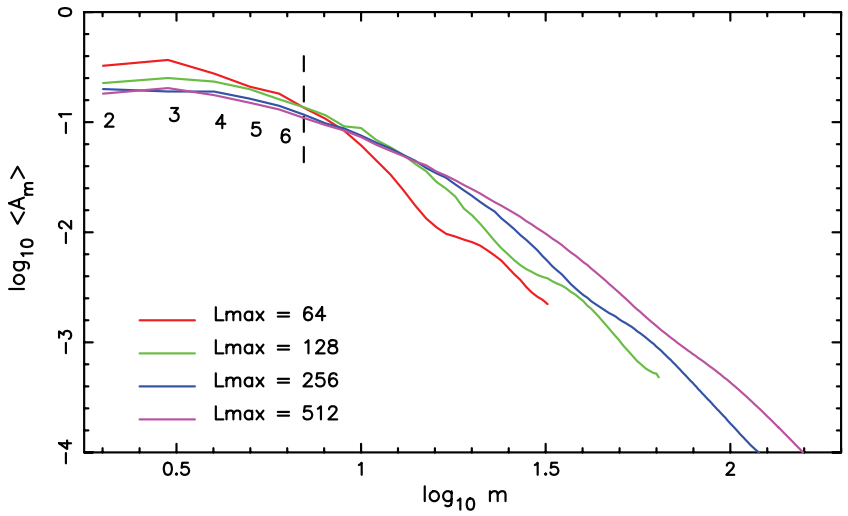

Figure 3. Logarithm of the amplitudes for the global Fourier components of the non-axisymmetric density structure plotted for different m-values. Note that the components with the highest global amplitudes are those with low m-values; $m = 2$–6 are labeled. The vertical dotted line corresponds with $m = 7$. For modes with $m < 7$, the radial range $\Delta r_{\rm LR}$ from the inner Linblad resonance to the outer Linblad resonance exceeds the disk scale height; the $\Delta r_{\rm LR}$ and scale height are roughly equal for $m = 7$.

(A color version of this figure is available in the online journal.)

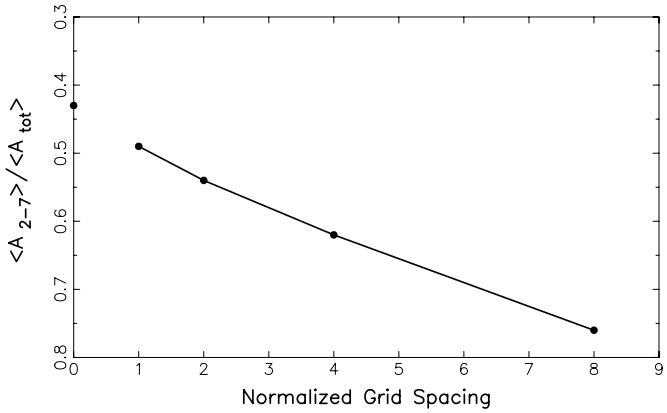

Figure 4. Convergence of the fractional amplitude of low-order non-axisymmetric structure. The x-axis represents the azimuthal "spacing" between grid points, normalized such that spacing of the $l_{\rm max} = 512$ grid equals unity. The y-axis displays the fraction of the total power in the low-order ($m = 2$–7) Fourier modes. Also plotted is the Richardson extrapolation for the asymptotic value $\langle A_{2\text{–}7}\rangle/\langle A_{\rm tot}\rangle = 0.43$ as the grid spacing goes to zero.

disk will decrease as $l_{\rm max}$ is increased. This can be tested by examining the torque contributions from various Fourier components.

The torque $\mathbf{C}$ on a cylindrical surface of the disk at radius ϖ can be obtained by integrating the stress tensor T over the surface of the cylinder (Lynden-Bell & Kalnajs 1972; Boley et al. 2006), i.e.,

$$\mathbf{C} = \int \mathbf{r} \times T \cdot dS. \tag{4}$$

If the stress tensor includes only gravitational stresses, the surface integral can be replaced with the volume integral

$$\mathbf{C} = \int \rho \mathbf{r} \times \nabla \Phi dV, \tag{5}$$

where Φ is the gravitational potential. Here we are interested only in the z-component of torque,

$$\mathbf{C}_Z = \int \rho \frac{\partial \Phi}{\partial \phi} dV, \tag{6}$$

as only this component drives mass and angular momentum transfer. The torque contribution from each mode m can be calculated by replacing ρ in Equation (6) with the density distribution reconstructed from a single Fourier component

$$\rho_m = a_{\phi m} \cos(m\phi) + b_{\phi m} \sin(m\phi), \tag{7}$$

where $a_{\phi m} = (1/\pi) \int \rho \cos(m\phi) d\phi$ and $b_{\phi m} = (1/\pi) \int \rho \times \sin(m\phi) d\phi$, and only the gravitational potential produced by the mass distribution given by ρ_m is included in Φ. Note that, as defined here, ρ_m is a function of ϖ, z, and ϕ while $a_{\phi m}$ and $b_{\phi m}$ are functions of ϖ and z.

Figure 5 displays time-averaged torques summed over a number of low-order modes, $\sum_1^n \langle \mathbf{C}_{Z(n)} \rangle$, $n = 1$, 2, 3, 4, and 5, and $\langle \mathbf{C}_{\rm Ztot} \rangle$, the total time-averaged gravitational torque arising from modes 1 through $l_{\rm max}/2$ as a function of radius and azimuthal resolution. The scale of the y-axis in each subplot is the same, with the exception of the $l_{\rm max} = 64$ simulation, where the scale is doubled. Because the star's position is artificially fixed at the center of the computational grid, torques arising from the $m = 1$ mode, typically 5%–10% of the total torque when averaged over the radial range of the figure, should not be considered realistic. Michael & Durisen (2010) found that freeing the star changes the torques by about 10%–20%, thus the difference between torques arising from the $m = 1$ mode with the star fixed and free to move are small compared to the differences found when comparing azimuthal resolution. In fact, it is expected that the $m = 1$ mode would only be effective at higher disk-to-star mass ratios (Shu et al. 1990).

We note two results in Figure 5: (1) the total gravitational torque is smaller for higher-resolution simulations and (2) the total torque is dominated by low-order Fourier components for all azimuthal resolutions. Both reflect the fact that while a higher fraction of the total power in larger $l_{\rm max}$ simulations is in higher-order m-values, these structures make only minimal contributions to the gravitational torque. As resolution increases, non-axisymmetric amplitude is shifted from low-order global components, which produce relatively large gravitational torques, to high-order local structures, which tend to cancel each other when integrated over the whole disk.

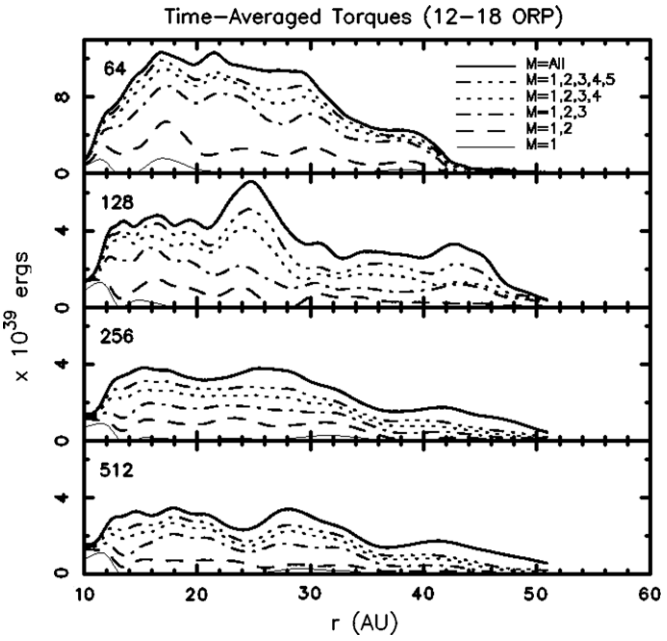

Figure 5. Total time-averaged gravitational torques, along with contributions arising from torques summed over combinations of $m = 1, 2, 3, 4$, and 5, as a function of radius and azimuthal resolution. Higher-resolution simulations are subject to smaller total torques while the total torque is dominated by low-order m-value components for all azimuthal resolutions. While a higher fraction of the total power in larger $l_{\max}$ simulations is in higher-order m-values, these components make only minimal contributions to the gravitational torque.

3.3. Effective Alphas

After obtaining the gravitational stresses in the disk, one can compute an effective α. Following Gammie (2001), Lodato & Rice (2004), and Boley et al. (2006),

$$\alpha_{\rm eff}(\varpi) = \left|\frac{d\ln\Omega}{d\ln\varpi}\right|^{-1} \frac{T^{\rm grav}_{\varpi\phi} + T^{\rm Reyn}_{\varpi\phi}}{\Sigma c_s^2}, \quad (8)$$

where Ω is the azimuthally averaged rotation speed, $T^{\rm grav}_{\varpi\phi}$ and $T^{\rm Reyn}_{\varpi\phi}$ represent the gravitational and Reynolds stress tensors, respectively, Σ is the surface density, and c_s is the sound speed. In comparison to Gammie's 2D models, the models studied here have a significant vertical extent. Because of this, the sound speed can vary dramatically from the mid-plane to the low-density regions. In order to include contributions to the sound speed from the entire vertical extent, the denominator Σc_s^2 was evaluated as $\int_z \rho c_s^2 dz$.

As discussed in Section 3.4, numerical uncertainties render Reynolds stresses difficult to determine accurately. This difficulty is mitigated somewhat by the fact that previous global 3D studies have found Reynolds stresses to be small relative to gravitational stresses (see, for example, Figure 5 of Lodato & Rice 2004 and Figure 10 of Boley et al. 2006). Here we omit $T^{\rm Reyn}_{\varpi\phi}$ from the calculation of $\alpha_{\rm eff}$ and show in Section 3.4 that, in fact, the gravitational torques are sufficient to account for all the mass transport. We note that Gammie (2001) found Reynolds and gravitational stresses contributed equally to $\alpha_{\rm eff}$ in his study. However, his was a local, shearing-sheet, 2D study. As such, it was unable to capture global effects, such as those seen in the cited 3D studies.

The gravitational stresses of Equation (8) can be evaluated using the gravitational torque of Equation (6), i.e.,

$$T^{\rm grav}_{\varpi\phi}(\varpi) = \frac{1}{2\pi\varpi^2} C_Z = -\frac{1}{2\pi\varpi^2}\int \rho \frac{\partial\Phi}{\partial\phi} dV. \quad (9)$$

Figure 6 shows $\alpha_{\rm eff}$, time-averaged from 12 to 18 ORPs, calculated using Equations (8) and (9), for the four grid resolutions. For comparison, $\alpha_{\rm eff}$ predicted by Equation (1) from Gammie (2001) are plotted for disks. The lower Gammie curve applies for the strongly self-gravitating limit while the upper curve represents the non-self-gravitating limit. The $l_{\max} = 512$ curve is consistent with these two limits. However, the $l_{\max} = 512$ curve does not represent a converged model. To determine whether the converged value of $\alpha_{\rm eff}$ is consistent with predictions, we examine the spatially (10–40 AU) and temporally (12–18 ORPs) averaged $\alpha_{\rm avg}$, provided in Table 1, for each value of $l_{\max}$. A Richardson extrapolation applied to these values converges to $\alpha_{\rm avg} = 0.017$ (over the same radial and time range) as the grid spacing goes to zero. This falls between the $\alpha_{\rm avg}$ values for the Gammie curves 0.014 (strongly self-gravitating) and 0.027 (non-self-gravitating).

At first glance, these results suggest strong agreement with Gammie and thus strong support for dissipative locality and GIs acting as a local mechanism overall. However, several cautionary notes are in order. It is important to remember that the bulk of the gravitational torque, and therefore the $\alpha_{\rm eff}$, is generated by low-order Fourier components that are coherent over tens of AU. As Table 1 shows, even at the highest resolution, where the relative strength of low-order structures is smallest, $\langle A_{2-7}\rangle$ accounts for half of the total amplitude. In order to accurately measure and characterize the contribution from these modes, one must consider a significant fraction of the disk. Even when averaged over 6 ORPs, Figure 6 shows that $\alpha_{\rm eff}$ displays $\sim$100% spatial fluctuations over a few AU. Furthermore, simulations of disks with a larger radial extent, e.g., hundreds of AU (Boley 2009), show coherent low-order modes over a significant fraction of the disk. In order to determine the radial extent and strength of such modes, one should consider the entire range of radii over which the disk is susceptible to instabilities, i.e., $Q \lesssim 1.5$ (Figure 1). In this context, Balbus & Papaloizou (1999) argue that a self-consistent local-disk picture, as required for a proper α-disk formulation, is probably not possible for GI-unstable disks, except perhaps near the corotation radius of a spiral wave. For the lowest-order modes in our disk, this is approximately centered at $\sim$25 AU.

In order to compare an $\alpha_{\rm eff}$, Gammie's formula, presented in Equation (1), also requires knowledge of the cooling time. This is generally not known a priori for a given disk. Moreover, the cooling time may not be easily parameterized with a local or global prescription over the entire disk. Simulations with realistic radiative physics (Boley et al. 2006) have shown that cooling times can vary substantially as a function of both radius and time in a GI active disk. In fact, it is these areas where the cooling rates change, leading to more or less GI activity, where many interesting phenomena may occur. In addition, at any given radius, the stresses, and hence $\alpha_{\rm eff}$, are highly variable with time. Figure 7 shows the time-variability of $\alpha_{\rm eff}$, normalized to its average value between $t = 14$ and 18 ORPs, at seven radial locations for times later than 12 ORPs. Here the time axis is normalized to the orbital time. Because the orbital periods are nearly Keplerian, at smaller radii the disk is followed for

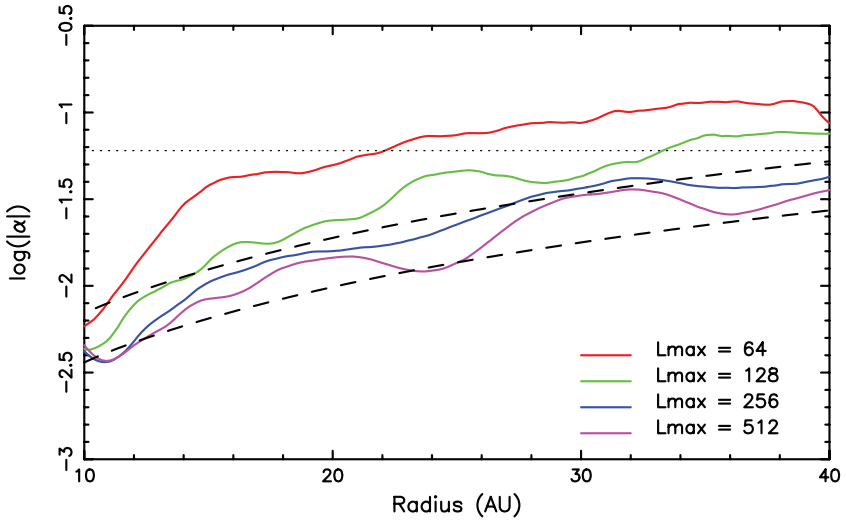

Figure 6. Effective α values for the $t_{\rm cool} = 2$ ORPs, $\gamma = 5/3$, $\Sigma \sim r^{-1}$ disk, averaged between 12 and 18 ORPs, for four different azimuthal grid resolutions, given by the number of azimuthal grid points $l_{\rm max}$. The dashed lines show the α from Equation (1) (upper: strongly self-gravitating limit, lower: non-self-gravitating limit), while the dotted line at $\log(\alpha) = -1.22$ represents the maximum stress a disk can maintain without fragmenting according to Rice et al. (2005).

(A color version of this figure is available in the online journal.)

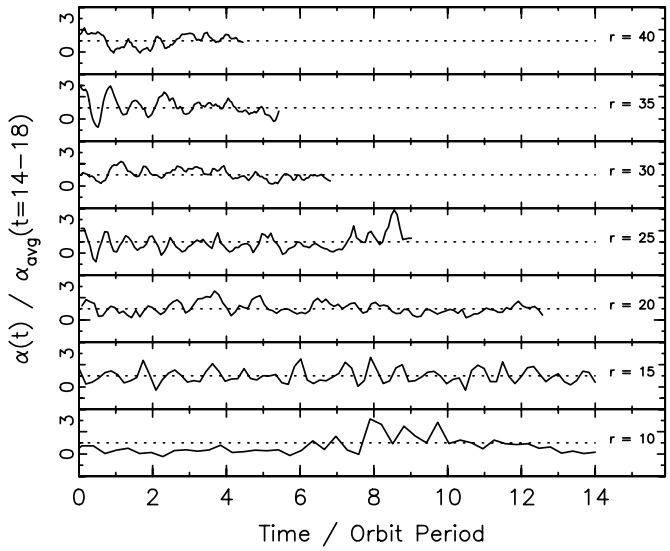

Figure 7. Local value of α at seven radii shown as a function of the local dynamical time. For radii greater than 20 AU, the plot shows the variation from 12 to 18 ORPs. At 10 and 15 AU, the 14 orbit periods immediately prior to 18 ORPs are shown. Dotted lines at an ordinate value of unity represent the average from 14 to 18 ORPs at that radius. Note that the local α displays $\sim$100% variations on the local dynamical time.

many more dynamical times than at larger radii. For ease of comparison, only the last 14 orbits are shown for $r = 10$ and 15. Fluctuations in $\alpha_{\rm eff}$ on the order of 100% or more are seen at all radii on timescales characteristic of the local dynamical time, indicating that this variability about the average is local in nature. The temporal averaging of Figure 6 washes out this local variability. Thus, even in this highly GI-active region, Gammie's formula only seems valid over many dynamic times when averaged over a substantial volume of the disk.

3.4. Convergence and $l_{\rm max}$

The results above permit an assessment of appropriate azimuthal grids for the problem under consideration and similar problems. The $l_{\rm max} = 512$ simulation yields a value for $\alpha_{\rm avg}$ of 0.020. This overestimates the extrapolated converged value of $\alpha_{\rm avg} = 0.017$ by $\sim$18%. The $l_{\rm max} = 512$ simulation also overestimates the fractional power in the high-order ($m = 2$–7) modes by essentially the same percentage. However, it should be noted that the fractional difference between successive doubling of the resolution has decreased for $l_{\rm max} = 512$. From $l_{\rm max} = 64$ to 128 the fractional difference in $\alpha_{\rm avg}$ is 36%. This decreases to 26% for the jump from $l_{\rm max} = 256$ to 512. Furthermore, the converged value represents infinite azimuthal resolution, which is, of course, impossible to achieve in a fixed grid scheme.

In addition to the convergence of $\alpha_{\rm avg}$, Table 1 illustrates the convergence of the measured net inward mass transport rates $\dot{M}$ over the time interval 12–18 ORPs. We tabulate the value of $|\dot{M}|$ spatially averaged over 10–40 AU. The absolute value of the net $\dot{M}$ at each r is taken prior to the spatial average because $\dot{M}$ varies in sign with r. It is the magnitude of the typical net mass transport rates that we wish to compare. The $|\dot{M}|_{\rm avg}$ measurements show convergence similar to that of the $\alpha_{\rm avg}$ measurement based on the gravitational torques. This gives us confidence that no important contributions from Reynolds stresses are being overlooked. Moreover, we have used Equation (22) of Boley et al. (2006) to estimate mass inflow rates based on the measured gravitational torques and find that these torques are indeed sufficient to account for the measured $\dot{M}$.

The principal reasons for not including the contributions from the Reynolds stress are twofold.

1. As elucidated in the above paragraph, the gravitational torques are sufficient to account for the measured α and $\dot{M}$, and all three converge as resolution is increased. There does not appear to be an additional source of stress required to explain the observed mass transport.
2. It is difficult to measure the Reynolds stress accurately in a nonlocal, strongly nonlinear calculation. The difficulty arises from the fact that the Reynolds stress is typically defined as

$$R_{ij} = \rho u_i' u_j', \tag{10}$$

where u_i' and u_j' are the fluctuations in the velocity field. The fluctuating pieces of the velocity field are defined as $u_i' = u_i - u_i(\rm avg)$, but in a gravitationally unstable

disk with extended non-axisymmetric spiral structures, the proper definition of the "mean" flow, u_i(avg), is unclear.

In attempting to measure the Reynolds stresses, we tried using several different definitions for u_ϕ(avg) and obtained results that varied dramatically. We used several local averaging schemes as well as an azimuthal average. Although Reynolds stresses are presented for other global simulations (e.g., Lodato & Rice 2004), the precise methods used to determine the stress values are not always elucidated. Because of this, it is difficult to make a direct comparison. The particulars of the method chosen can have a significant effect on the computed values of the Reynolds stress.

Another consideration is the effect of r and z resolutions on the outcome of the simulation. In this study we have chosen to focus on azimuthal resolution because it has the greatest effect on resolving the non-axisymmetric structures responsible for producing the gravitational stresses. However, as one increases the azimuthal resolution, the radius at which the cells have roughly equal sides increases as well. Ideally, this should occur near the radial range where GIs are most active. For $l_{\rm max} = 512$, $\delta r = r\delta\phi$ at $\approx$13.5 AU, which is near the radius where GIs are active.

Both the gravitational torques and $\alpha_{\rm eff}$ are functions of the gravitational stresses within the disk. If the Reynolds stresses are, in fact, negligible relative to the gravitational stresses, then the percentage errors in the calculated torques and $\alpha_{\rm eff}$ that stem from limited azimuthal resolution should be the same. In this case, the $l_{\rm max} = 512$ simulation should also be expected to yield gravitational torques that are $\sim$18% larger than the converged torques. For comparison, the errors in the $l_{\rm max} = 256$ simulations would exceed 50%. For many problems of interest, results obtained using $l_{\rm max} = 512$ should provide reasonable agreement with results obtained with higher resolution. Although computationally expensive, simulations with even higher resolution in all directions and codes using different grid geometry would be worthwhile.

3.5. Fragmentation and Effective Alphas

Under certain conditions, GIs fail to self-regulate, allowing density perturbations to grow until clumps form from spiral structure (see Durisen et al. 2007 for references). Under isothermal conditions, fragmentation becomes very likely whenever Q drops below 1.4 (Tomley et al. 1991, 1994; Nelson et al. 1998; Mayer et al. 2002). When the effective adiabatic index is stiff due to inefficient cooling, shocks and mass transport can militate against fragmentation, even in disks with initially low Q values (e.g., Boley & Durisen 2008). To understand the degree of cooling required to effect clump formation in non-isothermal disks, Gammie (2001) studied the nonlinear behavior of GIs using a series of shearing sheet simulations. He showed that a gravitationally unstable disk is likely to fragment whenever the cooling time is less than half the local orbital period ($t_{\rm cool}\Omega = 3$). This work was followed by Rice et al. (2005), who used global 3D smoothed particle hydrodynamics (SPH) simulations and found that the fragmentation limit was dependent on the adiabatic index. For disks with $\gamma = 5/3$, they found fragmentation occurred whenever the local cooling time was less than the local orbital period. For $\gamma = 7/5$, the limit was twice the local orbital period. Rice et al. (2005) proposed that this fragmentation threshold was due to a maximum stress that can be exerted on a disk by gravitational torques. Using the $\alpha_{\rm eff}$ as defined in Equation (8), they found that fragmentation could occur whenever $\alpha_{\rm eff} \gtrsim 0.06$ (the dotted line in Figure 6). The difference between the cooling time threshold found by Gammie and the ones found by Rice et al. are not obviously at odds, as Gammie's study was conducted in 2D and used a 2D adiabatic index of 2.

Recently, these results have been called into question by Meru & Bate (2011a), who suggest that our understanding of the fragmentation criterion is based on simulations that have yet to converge. In particular, they find that fragmentation becomes increasingly likely for longer cooling times when the resolution in their 3D SPH simulations is increased, giving weight to the claims by, e.g., Boss (2009) that fragmentation is a robust result of disk instability. The Meru & Bate study uses a prescribed cooling such that $t_{\rm cool} = \beta\Omega^{-1}$, where Ω is the local orbital frequency and β is some global constant. This same cooling prescription was used in the Gammie and Rice et al. studies. The reason for the differences is unclear, and may not be simply a resolution effect (Lodato & Clarke 2011). For example, the Gammie work revealed the most stringent cooling criterion of all the $t_{\rm cool}$ fragmentation studies, and, due to the local approximation Gammie used, these simulations are also at very high resolution. Moreover, Mejía et al. (2005), who used grid-based simulations with the same code we use here, and Boley & Durisen (2008), who used radiative hydrodynamics simulations, also found results that are reasonably consistent with those of Gammie (2001), Rice et al. (2005), and Cossins et al. (2010). Very recent work by Paardekooper et al. (2011) supporting the Gammie fragmentation criterion suggests that convergence results for fragmentation may be sensitive to the presence of sharp edges and the manner in which fragmentation is approached.

The present convergence study does not address fragmentation directly, but there are several results that should be noted. First, although the total power in non-axisymmetric structure is roughly constant throughout the simulations, the average Q value increases with increasing resolution (Table 1). Because both fast cooling and a low Q are necessary for fragmentation, this suggests that the disk is becoming less susceptible to clump formation with increasing resolution. Second, the disks do not show a trend toward denser spiral structure as the resolution is increased which is seen by eye in Figure 2, and is quantified by the decrease in $\langle A_{2\text{–}7}\rangle$. The high-$m$ modes are increasing in power, but remain smaller than the low-m components. Third, our results show that as the resolution increases, the disk approaches a self-regulating state that is reasonably well described, in the time- and space-average sense, by an α-disk with the parameterization of Gammie (2001).

Some caution must be taken when applying our results generally. The structure of the disk at the time of the onset of GIs may have a large impact on fragmentation. For example, Boley (2009) found that for disks with the same mass and *total* mass accretion rate, the disk with the shallower density profile fragmented, while the other did not (see also Meru & Bate 2011b). The disks explored here evolve to a surface density profile of approximately $p = 5/2$ in the outer regions for $\Sigma \propto r^{-p}$, while those explored by Meru & Bate (2011a) have a shallower profile ($p = 1$), favoring fragmentation. In addition to disk structure, the thermal history of the disk also plays a role in the fragmentation threshold. Clarke et al. (2007) found that the fragmentation cooling limit is sensitive to the way the instability is approached. When the cooling time is decreased slowly, the fragmentation limit is pushed toward shorter cooling times than if a fast cooling time is suddenly prescribed.

Overall, the disks simulated here are converging toward a state of self-regulation as the resolution is increased, and do not show signs of becoming more susceptible to fragmentation.

4. SUMMARY

We conducted a convergence study of a protostellar disk subject to GIs to examine the distribution and amplitudes of non-axisymmetric density structures arising from GIs and the connection of these structures to gravitational torques, to the level which transport can be represented by a simple α-disk formulation, and to fragmentation. A 3D hydrodynamics code with self-gravity was used to follow a disk subject to a constant global cooling time during its asymptotic state, when heating and cooling are roughly in balance. Four simulations were conducted, identical except for the number of azimuthal grid points, $l_{\rm max} = 64$, 128, 256, and 512, used in the calculations.

A Fourier decomposition of the non-axisymmetric density structure in $\cos(m\phi)$, $\sin(m\phi)$ was performed in order to characterize the amplitude distribution, A_m, of azimuthal structures as a function of m. This and previous studies have shown that disks in the asymptotic state have power at all resolvable m-values. The maximum value of m is given by $m_{\rm max} = l_{\rm max}/2$. Therefore, simulations with larger $l_{\rm max}$ can spread the power over more Fourier components. We find that $\langle A_{\rm tot}\rangle$, the power summed over all m, is roughly the same for all resolutions. However, the distribution of power among the Fourier components is distinctly affected by $l_{\rm max}$. The fractional amplitude in low-order modes, $\langle A_{2\text{–}7}\rangle/\langle A_{\rm tot}\rangle$, where $\langle A_{2\text{–}7}\rangle$ is the sum over modes $m = 2$–7, decreases monotonically with increasing resolution. Over three-quarters of $\langle A_{\rm tot}\rangle$ resides in $m = 2$–7 for the $l_{\rm max} = 64$ simulation, while approximately half resides in these m-values when $l_{\rm max} = 512$. A Richardson extrapolation suggests a limiting value of $\langle A_{2\text{–}7}\rangle/\langle A_{\rm tot}\rangle \sim 0.43$ as $l_{\rm max} \rightarrow \infty$. The number of degrees of freedom available for power, $l_{\rm max}/2$, increases linearly with the resolution. Thus, Fourier amplitudes are naturally spread from lower order to higher order as the available m-values increase.

Non-axisymmetric density structures produce gravitational torques, driving radial flows of mass and angular momentum. While the total torque is dominated by low-order Fourier components for all azimuthal resolutions, the total time-averaged gravitational torque is smaller for higher-resolution simulations. This reflects the fact that while a higher fraction of the total power in larger $l_{\rm max}$ simulations is in higher-order Fourier components, these components make only minimal contributions to the gravitational torque. As $l_{\rm max}$ increases, non-axisymmetric amplitude is shifted from low-order global components, which produce relatively large gravitational torques, to high-order local structures, which tend to cancel each other when integrated over the whole disk.

The effective $\alpha_{\rm eff}$ was determined for each simulation under the assumption that Reynolds stresses are negligible relative to the gravitational stresses, as found in previous 3D studies. As is the case for gravitational torques, $\alpha_{\rm eff}$ decreases with increased resolution. Derived values of $\alpha_{\rm eff}$ versus radius for the highest resolution simulation, $l_{\rm max} = 512$, are consistent with predictions from an analytic local theory for thin disks by Gammie (2001), as is the converged $\alpha_{\rm eff} = 0.017$, time-averaged over the asymptotic phase and spatially averaged over the disk. The time and spatially averaged $\alpha_{\rm eff}$ obtained for the $l_{\rm max} = 512$ simulations overestimates the converged value by less than 20%. Gravitational torques for this same model differ with converged values by a similar amount. Locally determined values of $\alpha_{\rm eff}$ vary by factors of two or three throughout the disk on timescales characteristic of the local dynamical time. Thus, the predictions of Gammie are only valid over many dynamic times when averaged over a substantial volume of the disk.

Although not a goal of this work, our simulations can be used to comment on studies of fragmentation and clump formation. Previous work indicates that our disk should not fragment due to the long cooling times that we use (e.g., Gammie 2001; Rice et al. 2005; Mejía et al. 2005; Boley & Durisen 2008). However, some recent studies (e.g., Boss 2009; Meru & Bate 2011a) suggest that previously determined fragmentation criteria too restrictive due to poor resolution. We find here that as the resolution is increased, our disk approaches a self-regulating state that can be reasonably well described, in the time- and space-average sense, by an α-disk parameterization. The average Toomre Q also increases with increasing resolution, suggesting that the disk becomes less susceptible to clump formation as the resolution is increased. This is consistent with our simulations not showing a trend toward denser spiral structure with increasing resolution. Moreover, recent work by Paardekooper et al. (2011) showed that if a high cooling rate is approached slowly, the Gammie (2001) cooling criterion is recovered for all resolutions considered. We do note that they find non-convergence with resolution when sharp edges in disks are present, but as the authors suggest, this may be numerically driven (see also Lodato & Clarke (2011) on numerical convergence issues in regards to fragmentation). Overall, the disks simulated here are converging toward a state of self-regulation as the resolution is increased, and do not show signs of becoming more susceptible to fragmentation.

A future paper will address the issues presented in this work using a convergence study of GI-susceptible disks subject to radiative cooling with realistic opacities. This will allow us to address the generality of the results cited herein.

We thank the anonymous referee for very useful comments that substantially improved this manuscript. S.M. thanks NASA for the generous funding of the NASA Earth and Space Science Fellowship NNX07AU82H. This research was also supported in part by NASA Origins of Solar Systems grants NNG05GN11G and NNX08AK36G. The simulations and analysis herein were conducted on hardware generously provided by the Indiana University Information Technology Services and was supported by the National Science Foundation under grants ACI-0338618l, OCI-0451237, OCI-0535258, CNS-0521433, and OCI-0504075. This work was also supported in part by Shared University Research grants from IBM, Inc., to the Indiana University. This work used the Extreme Science and Engineering Discovery Environment (XSEDE), which is supported by National Science Foundation grant number OCI-1053575

REFERENCES

Balbus, S. A., & Papaloizou, J. C. B. 1999, ApJ, 521, 650
Boley, A. C. 2009, ApJ, 695, L53
Boley, A. C., & Durisen, R. H. 2008, ApJ, 685, 1193
Boley, A. C., Durisen, R. H., Nordlund, Å., & Lord, J. 2007a, ApJ, 665, 1254
Boley, A. C., Hartquist, T. W., Durisen, R. H., & Michael, S. 2007b, ApJ, 656, L89
Boley, A. C., Mejía, A. C., Durisen, R. H., et al. 2006, ApJ, 651, 517
Boss, A. P. 1984, MNRAS, 209, 543
Boss, A. P. 2002, ApJ, 576, 462
Boss, A. P. 2009, ApJ, 694, 107
Cai, K., Durisen, R. H., Boley, A. C., Pickett, M. K., & Mejía, A. C. 2008, ApJ, 673, 1138
Cai, K., Durisen, R. H., Michael, S., et al. 2006, ApJ, 636, L149

Christodoulou, D. M. 1991, ApJ, 372, 471
Clarke, C. J., Harper-Clark, E., & Lodato, G. 2007, MNRAS, 381, 1543
Cossins, P., Lodato, G., & Clarke, C. J. 2009, MNRAS, 393, 1157
Cossins, P., Lodato, G., & Clarke, C. J. 2010, MNRAS, 401, 2587
Durisen, R. H., Boss, A. P., Mayer, L., et al. 2007, in Protostars and Planets V, ed. B. Reipurth, D. Jewitt, & K. Keil (Tucson, AZ: Univ. Arizona Press), 607
Durisen, R. H., Cai, K., Mejía, A. C., & Pickett, M. K. 2005, Icarus, 173, 417
Durisen, R. H., Gingold, R. A., Tohline, J. E., & Boss, A. P. 1986, ApJ, 305, 281
Gammie, C. F. 2001, ApJ, 553, 174
Goldreich, P., & Lynden-Bell, D. 1965, MNRAS, 130, 125
Hachisu, I. 1986, ApJS, 61, 479
Kratter, K. M., Matzner, C. D., Krumholz, M. R., & Klein, R. I. 2010, ApJ, 708, 1585
Larson, R. B. 1984, MNRAS, 206, 197
Laughlin, G., & Bodenheimer, P. 1994, ApJ, 436, 335
Laughlin, G., Korchagin, V., & Adams, F. C. 1997, ApJ, 477, 410
Laughlin, G., Korchagin, V., & Adams, F. C. 1998, ApJ, 504, 945
Laughlin, G., & Rozyczka, M. 1996, ApJ, 456, 279
Lin, D. N. C. 1981, ApJ, 246, 972
Lin, D. N. C., & Pringle, J. E. 1987, MNRAS, 225, 607
Lin, D. N. C., & Pringle, J. E. 1990, ApJ, 358, 515
Lodato, G., & Clarke, C. J. 2011, MNRAS, 413, 2735
Lodato, G., & Rice, W. K. M. 2004, MNRAS, 351, 630
Lodato, G., & Rice, W. K. M. 2005, MNRAS, 358, 1489
Lynden-Bell, D., & Kalnajs, A. J. 1972, MNRAS, 157, 1
Mayer, L., Quinn, T., Wadsley, J., & Stadel, J. 2002, Science, 298, 1756
Mejía, A. C. 2004, PhD thesis, Indiana Univ.
Mejía, A. C., Durisen, R. H., Pickett, M. K., & Cai, K. 2005, ApJ, 619, 1098
Meru, F., & Bate, M. R. 2011a, MNRAS, 411, L1
Meru, F., & Bate, M. R. 2011b, MNRAS, 410, 559
Michael, S., & Durisen, R. H. 2010, MNRAS, 406, 279
Nelson, A. F., Benz, W., Adams, F. C., & Arnett, D. 1998, ApJ, 502, 342
Nelson, A. F., Benz, W., & Ruzmaikina, T. V. 2000, ApJ, 529, 357
Norman, M. L., & Winkler, K.-H. A. (ed.) 1986, in NATO Advanced Research Workshop on Astrophysical Radiation Hydrodynamics, (Boston, MA: Reidel), 187
Paardekooper, S.-J., Baruteau, C., & Meru, F. 2011, MNRAS, 416, L65
Paczynski, B. 1978, Acta Astron., 28, 91
Papaloizou, J. C., & Savonije, G. J. 1991, MNRAS, 248, 353
Pickett, B. K., Cassen, P., Durisen, R. H., & Link, R. 1998, ApJ, 504, 468
Pickett, B. K., Cassen, P., Durisen, R. H., & Link, R. 2000, ApJ, 529, 1034
Pickett, B. K., Durisen, R. H., & Davis, G. A. 1996, ApJ, 458, 714
Pickett, B. K., Mejía, A. C., Durisen, R. H., et al. 2003, ApJ, 590, 1060
Press, W., Teukolsky, S., Vetterling, W., & Flannery, B. 1992, Numerical Recipes in C (2nd ed.; Cambridge: Cambridge Univ. Press)
Pringle, J. E. 1981, ARA&A, 19, 137
Rice, W. K. M., Armitage, P. J., Bate, M. R., & Bonnell, I. A. 2003, MNRAS, 339, 1025
Rice, W. K. M., Lodato, G., & Armitage, P. J. 2005, MNRAS, 364, L56
Shakura, N. I., & Sunyaev, R. A. 1973, A&A, 24, 337
Shannon, C. 1984, Proc. IEEE, 72, 1192
Shu, F. H., Tremaine, S., Adams, F. C., & Ruden, S. P. 1990, ApJ, 358, 495
Stamatellos, D., & Whitworth, A. P. 2008, A&A, 480, 879
Tomley, L., Cassen, P., & Steiman-Cameron, T. 1991, ApJ, 382, 530
Tomley, L., Steiman-Cameron, T. Y., & Cassen, P. 1994, ApJ, 422, 850
Toomre, A. 1981, in Structure and Evolution of Normal Galaxies, ed. S. M. Fall & D. Lynden-Bell (Cambridge: Cambridge Univ. Press), 111
van Albada, G. D., van Leer, B., & Roberts, W. W., Jr. 1982, A&A, 108, 76
Vorobyov, E. I. 2010, New Astron., 15, 24
Vorobyov, E. I., & Basu, S. 2005, MNRAS, 360, 675
Vorobyov, E. I., & Basu, S. 2006, ApJ, 650, 956
Walch, S., Naab, T., Whitworth, A., Burkert, A., & Gritschneder, M. 2010, MNRAS, 402, 2253
Yang, S. X. 1992, PhD thesis, Indiana Univ.
Yorke, H. W., & Bodenheimer, P. 1999, ApJ, 525, 330
Yorke, H. W., Bodenheimer, P., & Laughlin, G. 1993, ApJ, 411, 274